

Kinematic Emergence of the Page Curve in a Local Transverse-Field Ising Model

Samuel J. W. Jones,^{1,*} M. Basil Altaie,¹ and Benjamin T. H. Varcoe¹

¹*School of Physics and Astronomy, University of Leeds, Woodhouse, Leeds LS2 9JT*

(Dated: 7th May 2026)

We present a controllable quantum spin-chain model that reproduces the Page curve (the rise-and-fall of bipartite entanglement expected in black-hole evaporation), using only local interactions and a kinematic reduction of subsystem size. Two transverse-field Ising chains are coupled to form a pure bipartite state; Hawking-like evaporation is implemented by dynamically shrinking the ‘system’ chain and enlarging the ‘environment’ chain, while unitary real-time evolution is simulated with matrix product state (MPS) tensor networks. The characteristic Page curve profile emerges robustly under this controlled subsystem resizing, and notably persists even when the explicit Hamiltonian coupling across the boundary is set to zero, demonstrating that shrinking Hilbert-space dimension alone can generate Page curve behaviour. We show that the detailed shape of the curve depends on internal information dynamics, where operation at criticality yields a smooth profile, whereas moving away from criticality distorts entanglement growth and decay. These results position locally interacting spin chains as a realistic platform for probing black-hole-inspired information dynamics on current quantum hardware.

I. INTRODUCTION

Black holes, formed from the gravitational collapse of massive bodies, are characterised by only three classical parameters: mass, charge, and angular momentum [1–3]. Wheeler interpreted Israel’s proof [1] to imply that any static, uncharged black hole must take the form of the Schwarzschild solution, which means that all other information about the collapsed matter becomes inaccessible behind the event horizon [4], he coined this the ‘no-hair theorem’. Hawking showed that, near the event horizon of a static black hole, quantum field modes split so that positive-energy components escape to infinity, while negative-energy components fall into the black hole [5–7]. This process causes black holes to emit thermal radiation, and behave like black bodies. As the Hawking radiation carries energy away, the black hole gradually loses mass and shrinks, ultimately evaporating entirely, apparently without releasing the information that had fallen behind the horizon.

In contrast to this, Page treated gravitational collapse as a unitary quantum-mechanical process in which the black hole and its surrounding radiation together form a pure bipartite state [8, 9]. It was argued that unitarity requires this combined system to remain pure throughout its evolution and that if the black hole eventually radiates away entirely, the final state of the radiation must also be pure. From this assumption, he showed that during the first half of the black hole’s lifetime, the entanglement between the black hole and its environment—measured via the von Neumann entropy—should increase as Hawking radiation carries degrees of freedom into the environment. However, once the black hole has lost roughly half of its initial degrees of freedom, the trend reverses and the entropy begins to decrease. This is because the diminishing black hole Hilbert space can no longer support

increasing entanglement. During the second half of the lifetime, the information is effectively returned to the environment. The resulting rise and fall of entropy is the Page curve, shown in Fig.1, and this characteristic behaviour serves as a key diagnostic indicator for this work.

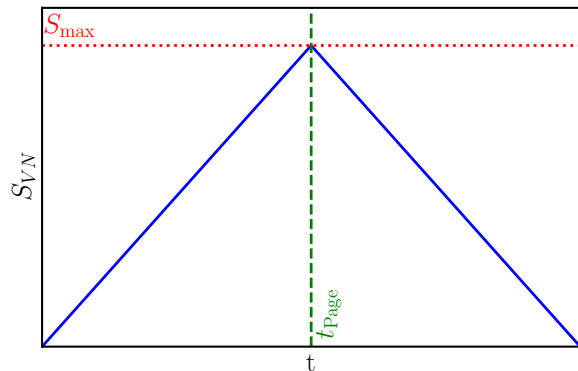


Figure 1. A Schematic of the idealised Page curve which depicts the behaviour of the entropy of the environment over time. Time is most intuitively defined as how much Hawking radiation has left the black hole until it eventually evaporates. In the first half of the black hole life, the entropy of the radiation grows and reaches a maximum until the growth is limited by the degrees of freedom present in the black hole Hilbert space. This turning point is the Page time. After this the entropy of the system decreases and information is recovered. This preserves unitarity and information within the system and is a proposed solution to the information paradox [9].

Given that Page has proposed a resolution to the apparent destruction of information in black-hole evaporation, our aim is to understand this mechanism more deeply and to probe how the Page curve actually emerges. Our goal is to construct a tangible model in which a system with decreasing degrees of freedom and non-trivial entanglement naturally reproduces the Page curve pro-

* ed20sjwj@leeds.ac.uk

file. The original argument presented in [8, 9] establishes a kinematic constraint based on subsystem dimensions, however it offers little guidance on how additional features, such as the internal information dynamics of the system, shape the entropy profile. We therefore seek a physically realisable analogue through which entanglement behaviour resembling that seen in Fig.1 can be investigated experimentally, motivated by the fact that pure quantum states are readily implemented in controllable spin-system platforms.

Page curve-like behaviour has been observed in a variety of Hamiltonian systems and is now an active area of research [10–14]. In these works the authors investigate the dynamics of fermionic chains in which the system portion is initially fully filled, and overtime it empties into an environment subsystem. This suggests that studying explicit Hamiltonian dynamics may reveal further insight into the conditions under which the Page curve arises and the constraints it imposes on entanglement evolution. Our work differs fundamentally from the work mentioned above in that we ensure a change in the number of degrees of freedom of each subsystem to more faithfully align with the initial derivation within [8, 9]. In this work, we study a microscopic toy model designed to probe entanglement dynamics in a controllable quantum many body setting. We implement a dynamic boundary condition that deterministically shrinks the system, creating an analogue of Hawking radiation that is motivated by the reduction of degrees of freedom as a black hole loses mass. Because Page’s original argument is fundamentally kinematic, the controlled subsystem resizing provides a faithful, and directly comparable analogue, to Page’s model.

The structure of this work is as follows, in Sec.II we provide the framework of the Hamiltonian and spin chain, which will directly move the degrees of freedom present in each subsystem. In Sec.III, we simulate the time evolution of this system and compute the von Neumann entropy of the system at each time step, showing that the entropy profile reproduces the Page curve as illustrated in Fig.1. This demonstrates that shrinking the spin chain offers a robust platform for exploring entropy dynamics on current quantum hardware. Building on this foundation, Secs.IV and V investigate whether internal information dynamics and dynamic coupling across the boundary are necessary to generate the required behaviour in the entropy. It is found that internal dynamics play an essential role in the form of the entropy profile noting suppression in the entropy growth in certain cases. An additional dynamic coupling beyond the kinematic boundary shift is not required. In the limit where the dynamic coupling is reduced to zero, leaving only the change in degrees of freedom, the characteristic Page curve remains.

II. MODEL

We utilize the Quantum Transverse Field Ising Model (TFIM) [15–22], which is comprised solely of local interactions. The TFIM is one of the most thoroughly understood frameworks in quantum many-body physics, with extensive research supporting its experimental realization in systems such as trapped ions and quantum hardware [22–25]. We look to probe the internal information dynamics of this system by initialising the system, and the environment, in and out of criticality such that we observe differing correlation lengths whilst maintaining experimental feasibility on superconducting chips or in trapped ion systems. A common choice of Hamiltonian to capture complex information dynamics (expected of a black hole [26]) would be the Sachdev-Ye-Kitaev (SYK) model often used in holographic dual models of gravitational systems [27]. The SYK model makes use of non-local ‘all-to-all’ interactions which facilitate extremely fast information propagation. However, this complexity often makes the system difficult to realize experimentally. Furthermore, such non-local interactions are not a strict requirement for the faithful reproduction of the Page curve [10–13]. As demonstrated in Sec.V, internal information dynamics play a critical role in the shape of the entanglement profile; however, the specific non-local dynamics of the SYK model are not a prerequisite. This suggests that a locally interacting model is sufficient to probe Page curve-like behaviour. The chain we model is a bipartite model partitioned into a system of length N and an environment of length M , with the sites ordered linearly see Fig.2. We employ the TFIM to perform an out-of-equilibrium quench, initializing the system in a non-eigenstate to drive internal dynamics. To mitigate finite-size boundary effects and facilitate the dissipation of entanglement from the system, we impose the condition $M \gg N$; specifically, we utilize $N = 15$ and $M = 150$ as our primary simulation basis. As detailed in Sec.III, we vary N to demonstrate that the observed Page curve dynamics scale consistently with increasing system size. The chain is then governed by the Hamiltonian given by

$$\hat{H} = \hat{H}_{sys} + \hat{H}_{env} + \hat{H}_{int}. \quad (1)$$

With the terms defined by

$$\begin{aligned} \hat{H}_{sys} &= -J_{sys} \sum_{i=1}^{N-1} \hat{\sigma}_i^z \hat{\sigma}_{i+1}^z - g_{sys} \sum_{j=1}^N \hat{\sigma}_j^x, \\ \hat{H}_{env} &= -J_{env} \sum_{i=N+1}^{L-1} \hat{\sigma}_i^z \hat{\sigma}_{i+1}^z - g_{env} \sum_{j=N+1}^L \hat{\sigma}_j^x, \\ \hat{H}_{int} &= -h \hat{\sigma}_N^z \hat{\sigma}_{N+1}^z. \end{aligned}$$

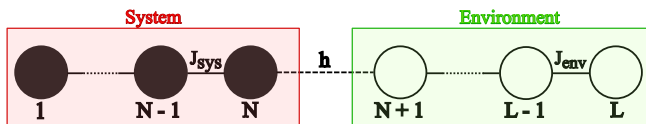


Figure 2. A schematic of the full spin chain modelled by the Hamiltonian given in Eq.1. The chain is split, one for the system coloured in red, of size N with interaction strength J_{sys} and one for the environment, in green, with interaction strength J_{env} and has length M . The overall size of the system is $L = N + M$ with a Hilbert space of size $\mathcal{H} \sim d^L$. The two subsystems are coupled with dynamic coupling h . To simulate evaporation we systematically move the dynamic coupling h to the left to grow the environment and decrease the system whilst allowing the system to naturally evolve through time using a TEBD protocol (see Appendix A for more information) to simulate unitary evolution.

To initialize the system at criticality: we set $J_{sys} = g_{sys}$, which maximizes the correlation length within the bounds established by the Lieb-Robinson velocity [28, 29]. Similarly, we set $J_{env} = g_{env}$ to ensure a gap-less environment. We impose the initial condition $J_{sys} > J_{env}$ to create an energy contrast, allowing the system to act as a higher-energy manifold relative to the environment. Furthermore, the transverse field is scaled as $h = \mathcal{O}(J_{sys})$; these combined conditions are designed to suppress the re-entry of information into the system chain once it has dissipated into the environment. A pure state $\hat{\rho}$ must satisfy the idempotency and normalization identities

$$\hat{\rho}^2 = \hat{\rho} \quad \text{and} \quad \text{tr}(\hat{\rho}^2) = 1, \quad (2)$$

where $\hat{\rho} = |\psi\rangle\langle\psi|$. Given that the derivation outlined in [8, 9] relies on the purity of the total system, both the system and environment subsystems are initialized in pure states. The global initial state is defined as

$$|\psi_I\rangle = |\zeta\rangle \otimes |\phi_0\rangle, \quad (3)$$

where the system state is

$$|\zeta\rangle = |0\rangle^{\otimes \frac{N}{2}} \otimes \frac{1}{\sqrt{2}} \left(|0\rangle^{\otimes \frac{N}{2}} + |1\rangle^{\otimes \frac{N}{2}} \right). \quad (4)$$

The environment state $|\phi_0\rangle$ is the state corresponding to E_0 , satisfying $\hat{H}_{env}|\phi_n\rangle = E_n|\phi_n\rangle$, where $E_0 = \min(\{E_n\})$. This choice of $|\phi_0\rangle$ mimics a vacuum-like environment by minimizing internal dynamics. The construction of $|\zeta\rangle$ accounts for the fact that black holes possess an entropy proportional to the surface area of their event horizon [30]. To satisfy the requirement for initial entanglement within a pure state, we utilize the Greenberger-Horne-Zeilinger (GHZ) state, $|GHZ\rangle = \frac{1}{\sqrt{2}}(|0\rangle^{\otimes n} + |1\rangle^{\otimes n})$ [31]. By initializing half the system in a GHZ state and the remainder as a product state, we localize the entanglement in a manner consistent with [30]. Standard unitary evolution with static subsystem sizes

fails to capture the loss of degrees of freedom characteristic of Hawking radiation. In physical evaporation, the continuous release of radiation reduces the black hole's mass and the dimension of its associated Hilbert space. To model this, we implement a dynamic boundary condition that discretely transfers spins from the system to the environment. The time-dependent subsystem lengths, $N(t)$ and $M(t)$, are governed by

$$N(t) = N_I - \left\lfloor \frac{t}{T} \right\rfloor, \quad (5)$$

and

$$M(t) = M_I + \left\lfloor \frac{t}{T} \right\rfloor, \quad (6)$$

where T represents the evaporation interval. This ensures that the system shrinks only at discrete steps $t = nT$ for $n \in \mathbb{Z}$, providing a computational dual to the decrease in Bekenstein-Hawking entropy [5]. The resulting time-dependent Hamiltonian is

$$\begin{aligned} \hat{H}(t) = & -J_{sys} \sum_{i=1}^{N(t)-1} \hat{\sigma}_i^z \hat{\sigma}_{i+1}^z - g_{sys} \sum_{j=1}^{N(t)} \hat{\sigma}_j^x \\ & - J_{env} \sum_{i=N(t)+1}^{L-1} \hat{\sigma}_i^z \hat{\sigma}_{i+1}^z \\ & - g_{env} \sum_{j=N(t)+1}^L \hat{\sigma}_j^x - h \hat{\sigma}_{N(t)}^z \hat{\sigma}_{N(t)+1}^z. \end{aligned} \quad (7)$$

While $\hat{H}(t)$ is globally time-dependent, the Hamiltonian remains piecewise constant between evaporation events. This allows for standard unitary propagation within each interval T , followed by a discrete update of the subsystem boundaries. The simulation of large-scale quantum systems is constrained by the exponential scaling of the Hilbert space, $\mathcal{H} \sim d^L$. Direct diagonalization of \hat{H}_{env} becomes intractable as M increases. To circumvent this dimensionality problem, we employ MPS, a tensor network formalism that decomposes the high-order state tensor into a chain of low-rank local tensors [32, 33].

III. THE PAGE CURVE

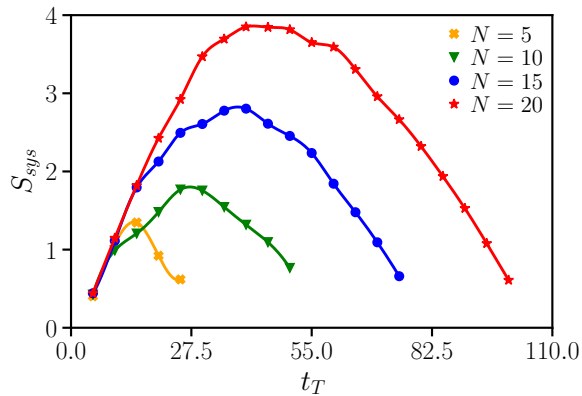


Figure 3. We simulate time evolution of the time independent Hamiltonian \hat{H} through unitary evolution simulated with a TEBD protocol (see Appendix A for more information). The x-axis denotes the time evolution passed, simulated in increments of $\tau = 0.1$ with an evaporation time-step $T = 5$, each marker denotes a point where an evaporation event was performed. When $\frac{t}{T} \in \mathbb{Z}$ the von Neumann entropy is measured, recorded and then an evaporation event is performed. The result is the von Neumann behaves in alignment with the Page curve after around half the time has passed (the Page time) the entropy decreases due to being limited by the size of the system since Eq.8 holds for the bipartite model. N is denoted in the differing colours and can be seen in the figure. The rest of the parameters are as follows: $J_{sys} = g_{sys} = h = 3$, $J_{env} = g_{env} = 1$ and $M = 150$.

In Fig.3, the calculated entropy is shown over the entire simulated evaporation process. The characteristic rise and fall of the Page curve (idealized in Fig.1) is present, with the turnover occurring when the subsystems are approximately equal in size. We thus observe entanglement behaviour consistent with the dimensional constraints of a unitary bipartite model undergoing subsystem reduction. We note an asymmetry in the gradient about the Page time, arising from the different mechanisms dominating early versus late times. During the early stages, the system is dominated by information transfer, characterized by the interaction strengths and the dynamic coupling h , which determines the rate of entanglement growth. Conversely, after the Page time, the system size dominates the environment entropy. The limited degrees of freedom in the system restrict the entropy in accordance with von Neumann behaviour for a pure bipartite model where

$$S_{env} = -\text{tr}_{env}(\hat{\rho}_{env} \ln \hat{\rho}_{env}) \equiv S_{sys}. \quad (8)$$

While these behaviours need not have the same rate of change, they could be fine-tuned via parameters if necessary. At $t = 0$, the environment begins in its ground state with its associated entanglement. At the final time-step when $N = 0$, the simulation does not record the entropies. This is an artifact of measuring the von Neumann

entropy just before an evaporation event. After the final spin leaves the system, the entropy is zero by definition, as seen from Eq.8 since $\hat{\rho}_{sys} = 0$. Thus, the entropy begins and ends at zero, conserving information. This confirms that the Hamiltonian is sufficient to realize entanglement dynamics consistent with Fig.1, providing a platform to probe how dynamic coupling and internal dynamics affect the Page curve.

IV. THE EFFECT OF THE DYNAMIC COUPLING h

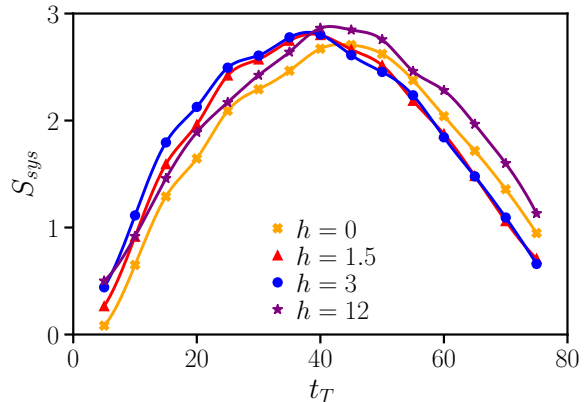


Figure 4. We simulate time evolution of the time independent Hamiltonian \hat{H} through unitary evolution simulated with a TEBD protocol (see Appendix A for more information). The x-axis denotes the time evolution passed, simulated in increments of $\tau = 0.1$ with an evaporation time-step $T = 5$, each marker denotes a point where an evaporation event was performed. When $\frac{t}{T} \in \mathbb{Z}$ the von Neumann entropy is measured, recorded and then an evaporation event is performed. Note when the dynamic coupling between the system and the environment $h = 0$, there is still a characteristic rise and fall throughout the entire process when the system is entirely kinematic. Since there is no dynamic coupling between the two subsystem when $h = 0$ the Page curve is purely down to the kinematic transfer of the degrees of freedom. We see that having no dynamic coupling has little effect on the entropic behaviour. The variations of h are denoted in the differing colours and can be seen in the figure. The rest of the parameters are as follows: $J_{sys} = g_{sys} = 3$, $J_{env} = g_{env} = 1$, $N = 15$ and $M = 150$.

In Fig.4, we observe the effects of the dynamic coupling between the two subsystems throughout the evaporation process. We conclude that the dynamic coupling h plays a secondary role in shaping the entropy profile of the Page curve, as there is no discernible correlation between the peak of S_{VN} and differing values of h . This implies that the kinematic process remains the primary driver of the entropy evolution. When $h = 0$, there is no dynamic information transfer across the boundary mediated by the Hamiltonian; instead, transfer is governed solely by the kinematic evaporation process that imposes the analogue

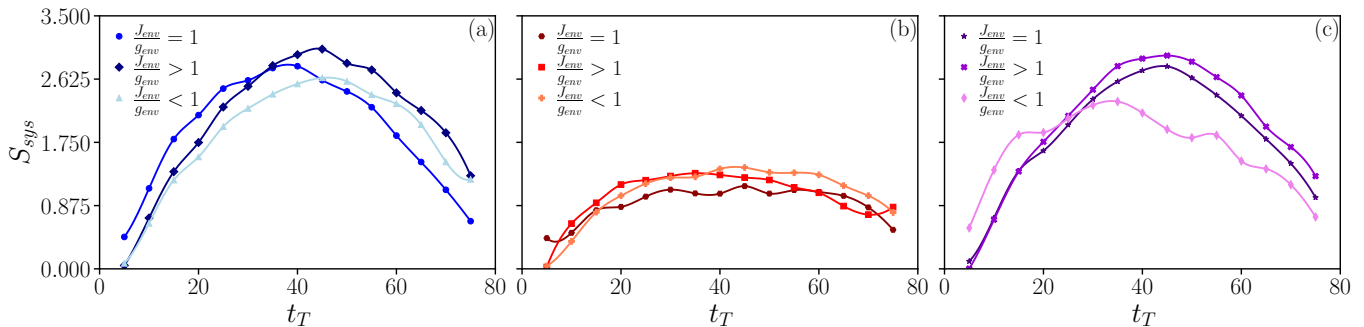


Figure 5. We simulate time evolution of the time independent Hamiltonian \hat{H} through unitary evolution simulated with a TEBD protocol (see Appendix A for more information). In this plot we vary the relationships $\frac{J_{sys}}{g_{sys}}$ and $\frac{J_{env}}{g_{env}}$ to probe how criticality effects the outcome of the entropy profile. The x-axis denotes the time evolution passed, simulated in increments of $\tau = 0.1$ with an evaporation time-step $T = 5$, each marker denotes a point where an evaporation event was performed. We keep $N = 15$, $M = 150$ and $h = 3$. When $\frac{t}{T} \in \mathbb{Z}$ the von Neumann entropy is measured, recorded and then an evaporation event is performed. We ran this simulation for each permutation of the system and environment subsystems being governed by the Hamiltonian with $\frac{J}{g} > 1, \frac{J}{g} < 1$ or $\frac{J}{g} = 1$. These permutations are categorised above into three subplots, the data is grouped via the conditions imposed on the system with (a) being when the system is at criticality, (b) when $J_{sys} > g_{sys}$, and (c), when $J_{sys} < g_{sys}$. We find in figure (b) that when the system has a large J then it significantly effects how entropy behaves within the environment when compared to the system at criticality. We observe a significant suppression in the entropy growth in the first half of the Page curve, which is dependent on the dominance of the J_{sys} .

Hawking radiation in this model. This kinematic process entails a time-dependent change in the degrees of freedom, representing a coupling that mimics the redistribution of entanglement as degrees of freedom exit the black hole horizon. The emergence of the Page curve at $h = 0$ demonstrates that explicit Hamiltonian-mediated information transfer is not a prerequisite for these dynamics. Instead, the entanglement profile is effectively captured by the kinematic resizing of the Hilbert space—a process that serves as a discrete analogue to the shifting degrees of freedom in Page’s original derivation.

V. THE EFFECT OF CRITICALITY

We have thus far found that an additional dynamic coupling, beyond the kinematic mechanism accounting for Hawking radiation, is not strictly necessary. We now provide insight into the effects of placing each subsystem in or out of criticality. Simulations were performed for the system and environment under three conditions: $\frac{J}{g} > 1$, $\frac{J}{g} < 1$, and $\frac{J}{g} = 1$. We find that when the condition $\frac{J}{g} > 1$ is imposed on the system, there is a significant variation in the von Neumann entropy such that it deviates from the characteristic rise and fall. This does not imply that information is no longer conserved; since the entropy begins and ends at 0, global information conservation is maintained. However, the deviation from smooth rise and fall suggests that internal information dynamics influence the entropy profile over time, meaning the entanglement evolution is not as cleanly captured. We infer from this that a minimum scrambling speed is required for the Page curve to be faithfully reproduced.

However, a perfect “fast scrambler” is not strictly required, as reproducing the characteristic entropy profile within the TFIM would otherwise have been impossible.

VI. A TOY QUANTUM CIRCUIT

Here we provide the quantum circuit for a system of $L = 6$ qubits, with $N = 4$ and $M = 2$, implementing the Hamiltonian defined in Eq.7 for a single Trotter step. We utilize a second-order Suzuki-Trotter decomposition [34] of the piecewise time-independent Hamiltonian, which accurately describes the evolution between discrete evaporation events. The time evolution is discretized into small steps τ , where $\tau \ll t_{total}$, and the decomposition is applied iteratively. When an evaporation event occurs, it is captured by updating the gate set: the interaction gates corresponding to the system-environment boundary are shifted, and the departing system qubit is thereafter treated with environment interaction gates. To implement this, the full Hamiltonian is decomposed into sums of local terms that can be exponentiated exactly. Because the $\hat{\sigma}^x$ and $\hat{\sigma}^z$ terms do not commute, they must be applied as a sequence of discrete unitary operators. Given that the Hamiltonian is composed entirely of local interactions, we express the second-order decomposition using alternating layers of even and odd bond interactions. This approach limits the circuit depth to four layers per Trotter step, enhancing computational efficiency. The specific form of the Trotter decomposition is determined by whether the current system size N is even or odd, ensuring the boundary coupling h is correctly localized at each step. The evolu-

tion is approximated as

$$\begin{aligned}
\hat{U}_{\text{odd}}(\tau) \approx & \prod_{i=1}^N e^{g_{\text{sys}} i \frac{\tau}{2} \hat{\sigma}_i^x} \prod_{i=N+1}^L e^{g_{\text{env}} i \frac{\tau}{2} \hat{\sigma}_i^x} \\
& \prod_{i=N+1}^L e^{J_{\text{sys}} i \tau \hat{\sigma}_{2i}^z \hat{\sigma}_{2i+1}^z} \prod_{i=1}^N e^{J_{\text{sys}} i \tau \hat{\sigma}_{2i}^z \hat{\sigma}_{2i+1}^z} \\
& \prod_{i=N+1}^L e^{J_{\text{env}} i \tau \hat{\sigma}_{2i-1}^z \hat{\sigma}_{2i}^z} \cdot e^{i h \tau \hat{\sigma}_N^z \hat{\sigma}_{N+1}^z} \\
& \prod_{i=1}^N e^{J_{\text{sys}} i \tau \hat{\sigma}_{2i-1}^z \hat{\sigma}_{2i}^z} \prod_{i=N+1}^L e^{g_{\text{env}} i \frac{\tau}{2} \hat{\sigma}_i^x} \\
& \prod_{i=1}^N e^{g_{\text{sys}} i \frac{\tau}{2} \hat{\sigma}_i^x}, \tag{9}
\end{aligned}$$

$$\begin{aligned}
\hat{U}_{\text{even}}(\tau) \approx & \prod_{i=1}^N e^{g_{\text{sys}} i \frac{\tau}{2} \hat{\sigma}_i^x} \prod_{i=N+1}^L e^{g_{\text{env}} i \frac{\tau}{2} \hat{\sigma}_i^x} \\
& \prod_{i=N+1}^L e^{J_{\text{env}} i \tau \hat{\sigma}_{2i}^z \hat{\sigma}_{2i+1}^z} \cdot e^{i h \tau \hat{\sigma}_N^z \hat{\sigma}_{N+1}^z} \\
& \prod_{i=1}^N e^{J_{\text{sys}} i \tau \hat{\sigma}_{2i}^z \hat{\sigma}_{2i+1}^z} \prod_{i=N+1}^L e^{J_{\text{env}} i \tau \hat{\sigma}_{2i-1}^z \hat{\sigma}_{2i}^z} \\
& \prod_{i=1}^N e^{J_{\text{sys}} i \tau \hat{\sigma}_{2i-1}^z \hat{\sigma}_{2i}^z} \prod_{i=N+1}^L e^{g_{\text{env}} i \frac{\tau}{2} \hat{\sigma}_i^x} \\
& \prod_{i=1}^N e^{g_{\text{sys}} i \frac{\tau}{2} \hat{\sigma}_i^x}. \tag{10}
\end{aligned}$$

This decomposition assumes the convention $\hbar = 1$. Quantum computers are susceptible to various noise sources and gate errors (see, for example, [35]). Consequently, simplifying circuit implementation is imperative to optimize performance on current quantum hardware. In the chosen decomposition, a brickwork architecture is employed: two-site operators initially act upon all odd-labelled pairs, followed by a layer of two-site operators acting upon all even-labelled pairs. This structure can be directly mapped to a quantum system using standard one- and two-qubit rotation gates.

The rotation-x gate angle is defined as ϕ , and the rotation-z gate angle as θ . These angles are directly related to the exponents in Eqs.9 and 10; due to the exponential form of the rotation operators, they are given by

$$\phi_{\text{sys,env}} = -\tau g_{\text{sys,env}}, \tag{11}$$

$$\theta_{\text{sys,env}} = -2\tau J_{\text{sys,env}}, \tag{12}$$

and

$$\theta_h = -2\tau h. \tag{13}$$

To initialize the environment: the ground state of \hat{H}_{env} is directly diagonalized, yielding a weighted Bell-type state. This state can be prepared using a rotation-y gate in conjunction with standard entangling operations. The system comprises 4 qubits, with the first two initialized in the $|0\rangle$ state and the remaining two in a maximally entangled state. This initialization sequence is shown in the first section of Fig.6. Subsequently, the figure illustrates a complete circuit for two Trotter steps; these steps are repeated for a total of n iterations to simulate a sufficient duration of the system dynamics. For a full model compatible with quantum hardware, an algorithm which can measure the entropy without de-cohering the system must be implemented. This is a matter which we leave to future work, noting some of the work in [36] may be useful.

VII. DISCUSSION

We assess the validity of a model composed strictly of local interactions. In the literature, the SYK Hamiltonian is frequently employed to simulate black hole information dynamics due to its fast-scrambling properties. In contrast, the model presented here utilizes the TFIM, which is constrained by local interactions and the Lieb-Robinson velocity. By operating the system at criticality, we demonstrate that the internal dynamics are sufficient to maintain the smooth entropy profile predicted by Page [8, 9]. As supported by the results in Secs.III-V, non-local interactions are not a strict requirement for reproducing Page curve-like entanglement dynamics in analogue toy models. Consequently, critical local systems are sufficient for this purpose and offer a more viable path for experimental verification on contemporary quantum hardware. The primary advantage of the TFIM is its compatibility with current quantum architectures as demonstrated by this model in Sec.VI. While ground-state initialization can be explored on quantum annealers [22, 37], the dynamic evaporation process is well-suited for gate-based quantum computers, such as those developed by IBM [38]. Specifically, the Trotter-Suzuki decomposition employed in our Time-Evolving Block Decimation (TEBD) simulations translates directly into sequences of one- and two-qubit gate operations. The locality of the interactions minimizes the requirement for SWAP gates during the implementation of the TEBD protocol, thereby reducing a primary source of gate noise and decoherence that would otherwise plague non-local models. Naturally, the question of how S_{VN} could be measured after various iterations of the circuit given in Fig.6 without invoking decoherence remains open as a logical next step. Also, quantifying the scrambling through established methods such as Out-of-time-order correlators (OTOCs) [39–44], and correlating the findings with those presented in Fig.5.

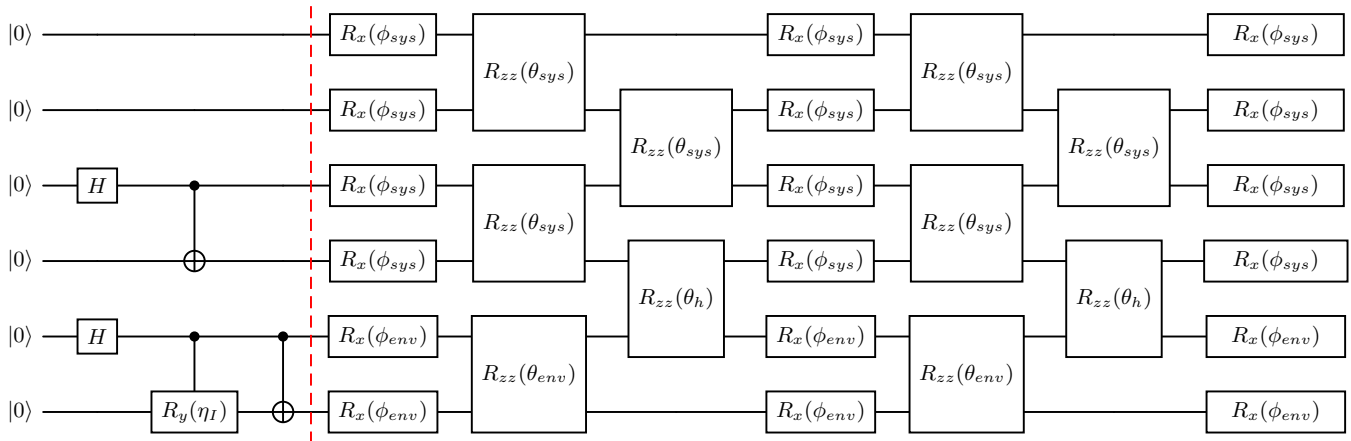


Figure 6. In this figure the quantum circuit for $L = 6$ with $N = 4$ being the first four qubits from the top, representing the system initialised in a half $|0\rangle$ and half entangled state. $M = 2$ are the bottom two qubits initialised in the ground state found via exact diagonalisation and with $\eta_I = 1.107$. The circuit is split into two parts, the first part initialises in the state found via diagonalisation for the environment and a system for the system where half is in the bell state and half the $|0\rangle$ state. The second part is two trotter step to simulate the time evolution of this system. depicted are two repetitions of this step. The angles of rotation are dependant on τ and the interaction strengths.

VIII. CONCLUSION

In this work, we have investigated the conditions under which Page curve-like entanglement dynamics emerge within local quantum many-body systems. Utilizing MPS simulations of a local, Ising-based Hamiltonian, we implemented a dynamic boundary condition to model the systematic reduction of subsystem degrees of freedom. Time evolution was executed via a TEBD algorithm employing a Suzuki-Trotter decomposition. The findings presented in Sec.IV demonstrate that explicit dynamical coupling between the system and environment is not a fundamental requirement for the manifestation of the Page curve. Even in the limit where the Hamiltonian coupling h vanishes, the characteristic rise and fall of the von Neumann entropy persist. While the existence of the Page curve is fundamentally kinematically driven, its specific profile remains sensitive to the internal dynamics of the subsystems. As shown in Sec.V, the smooth entropy profile is most faithfully reproduced when the system operates at criticality. Away from the critical point, deviations and suppression in the entropy profile suggest that the propagation of correlations—constrained by local interactions and the Lieb-Robinson bound—plays a critical role in the growth of entropy prior to the Page time. Consequently, we conclude that internal dynamics are crucial in determining the qualitative nature of the entropy evolution. This work establishes a scalable and experimentally feasible platform for further exploration of entanglement dynamics on near-term quantum hardware.

ACKNOWLEDGEMENTS

We would like to thank Jiannis Pachos for his insight into black hole simulations. S.J. would also like to acknowledge Ryan Smith and Max Davies for many stimulating and interesting discussions on various topics mentioned within this work. This work was partially supported by the EPSRC grant UKRI1337: Anyons24.

Appendix A: Methodology

The following method was implemented using ITensor.jl [45], unless stated otherwise throughout. We first designate our initial state as Eq.4. We do this by creating both $|\zeta\rangle$ on sites 0 to N and $|\phi_0\rangle$ on sites $N+1$ to L separately as MPS, and then introducing a bond of dimension 1 to connect them. For $|\zeta\rangle$ we initially create an MPS of $|0\rangle^{\otimes N}$ to which we apply a combination of Z and $CNOT$ gates to the appropriate spin sites, faithfully creating $|\zeta\rangle$. To create the ground state $|\phi_0\rangle$ we must first know what it actually is. Analytically, the ground state is found by exactly diagonalising the Hamiltonian matrix, however given the size of the matrix H_{env} scales exponentially with the Hilbert space, this becomes computationally intractable. Since the Hamiltonian is a sum of local terms, we may efficiently approximate the ground state through the Density Matrix Renormalization Group Algorithm (DMRG) [46–50]. The DMRG calculation was converged over 10 sweeps, achieving a maximum allowed bond dimension of $\chi = 100$ and a final truncation error of $\epsilon < 10^{-10}$. We note a convergence of the ground state at low bond dimension circa $\chi = 40$, this ensures the max-

imum allowed bond dimension of $\chi = 100$ is well suited to an accurate approximation of the ground state. From there we bonded the two systems together with $\chi = 1$ (a tensor product) creating no initial entanglement between the two subsystems which is expected from the form of Eq.4.

To simulate real-time evolution we implement a second algorithm: a TEBD algorithm [33, 34, 51]. Starting from the initial state $|\psi_T\rangle$, we use a second-order Trotter-Suzuki decomposition [33, 52] of the standard time independent evolution operator. It is permissible to not use the time dependent Trotter-Suzuki algorithm [53] since between evaporation events the Hamiltonian is time independent. In this case, the Trotter step was chosen to be $\tau = 0.1$ with a cut-off of $\epsilon = 10^{-5}$. At regular intervals when $\frac{t}{T} \in \mathbb{Z}$, where $T \gg \tau$, we calculate the von Neumann entropy of the environment system. The von Neumann entropy is given by

$$S_{VN} = - \sum_i \lambda_i \ln(\lambda_i), \quad (\text{A1})$$

where λ_i are the eigenvalues of the reduced density matrix found via the Schmidt decomposition of the environment. After this calculation, the lengths of each chain are redefined, such that $N \rightarrow N - 1$ and $M \rightarrow M + 1$, simulating Hawking radiation in this system. This is computationally realised by adjusting the Hamiltonian such that H_{sys} acts on one less spin site and H_{env} acts on one more spin site for the next evolution interval of T . The spins which are changed are the ones at the boundary, thus moving the dynamic coupling to the left in Fig.2, decreasing the system. The entropy at the end of the next interval is calculated in accordance with the new size of the environment. The system itself remains constant in its size of L .

Appendix B: Non-Unique Initial System State

We provide here the some of the results of a full simulation for an alternative initial state of the system to show that the dynamics presented in Secs.III and V were not solely down to the $|\zeta\rangle$ initialisation of the system. We first propose a more trivial initial state of

$$|\xi\rangle = |1\rangle^{\otimes N}, \quad (\text{B1})$$

where all the spins align and is easily verifiable from (5) to be a pure state. The initial state now becomes

$$|\psi'_T\rangle = |\xi\rangle \otimes |\phi_0\rangle, \quad (\text{B2})$$

where $|\phi_0\rangle$ retains its initial definition from Sec.II. After running the same TEBD protocol we find that the system provides similar results under varying $\frac{J}{g}$ conditions. The fact the Page curve is present for differing initial system states demonstrates the robustness of the kinematic model.

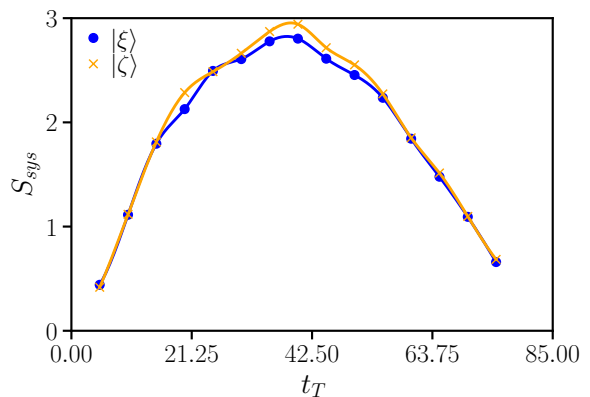


Figure 7. We track the entropy of two systems, one initialised in the entangled $|\zeta\rangle$ state and the other in the $|\xi\rangle$ state where all the spins are aligned. We find no quantitative difference in the behaviour, demonstrating the robustness of the model. The x-axis denotes the time evolution passed, simulated in increments of $\tau = 0.1$ with an evaporation time-step $T = 5$, each marker denotes a point where an evaporation event was performed. When $\frac{t}{T} \in \mathbb{Z}$ the von Neumann entropy is measured, recorded and then an evaporation event is performed. The rest of the parameters are as follows: $h = J_{sys} = g_{sys} = 3$, $J_{env} = g_{env} = 1$, $N = 15$ and $M = 150$.

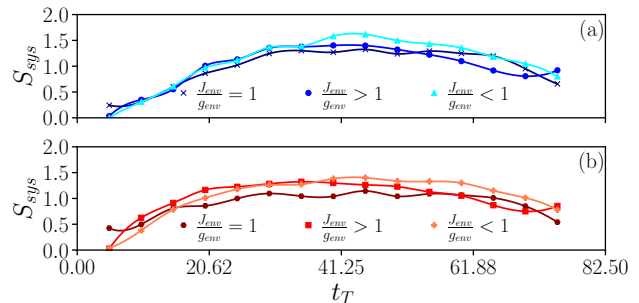


Figure 8. We track the entropy of two systems, the chain in (a) is initialised in the $|\xi\rangle$ state where all the spins are aligned whereas in figure (b) it is initialised in the $|\zeta\rangle$. We vary the ratio of $\frac{J_{env}}{g_{env}}$ whilst keeping $\frac{J_{sys}}{g_{sys}} > 1$. We find no quantitative difference in the behaviour with it being similar between the two initial states, demonstrating the robustness of the model. This verifies the initial states do not quantitatively effect the outcome and it is indeed the dynamics of the model. The x-axis denotes the time evolution passed, simulated in increments of $\tau = 0.1$ with an evaporation time-step $T = 5$, each marker denotes a point where an evaporation event was performed. When $\frac{t}{T} \in \mathbb{Z}$ the von Neumann entropy is measured, recorded and then an evaporation event is performed. The rest of the parameters are as follows: $J_{sys} = 10$, $h = g_{sys} = 3$, $N = 15$ and $M = 150$.

Appendix C: DMRG Convergence

We ensure we reach a convergence in the DMRG protocol to ensure an accurate ground state approximation

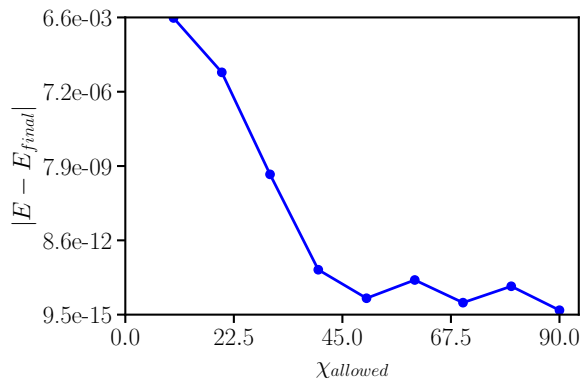


Figure 9. We plot the Maximum bond dimension allowed against the ground state energy error on a logarithmic scale. The energy is approximated through the DMRG algorithm. This convergence shows an accurate approximation was found at a relatively low which means we can increase computational capability by keeping the dimension low too. This convergence also ensures an accurate estimate for the initial state, reducing errors as the simulation progresses.

to begin the simulation. We show this by plotting the error in energy against maximum bond dimension allowed in the interaction. By doing so we ensure that the initial ground state approximation is accurate to an insignificant error. This reduces the size of errors accumulating throughout the time evolution steps. It also ensures that we can limit the size of the bond dimension used without affecting the system dynamics, this increases computational capability and allows for larger system sizes to be simulated. We observe a convergence of around $\chi \approx 45$ which is much less than the maximum bond dimension of 100 which we reached during the DMRG protocol. From this we conclude an accurate ground state was reached, minimising the error contribution from this approximation that is present in the overall simulation.

Appendix D: Variation of τ

In this section we plot the entanglement entropy of the environment for varying values of the trotter step to ensure the original choice of $\tau = 0.1$ is an accurate value to

approximate the behaviour of the Hamiltonian. In Fig.10 it can be seen that $\tau = 0.1$ provides a good approximation to the time evolution without becoming computationally too expensive to run. We see we can optimise this choice slightly by using a larger value $\tau = 0.5$ which provides qualitatively the same results for a better computing performance. We note there is a lower and upper bound to retrieving the Page curve dynamics which must be ensured when the value of τ is chosen. When τ is large (of the order of T) there has not been a sufficient number of steps to capture the entanglement growth faithfully, leading to a slower entanglement growth which is not peaking at around the Page time. Conversely, if τ is sufficiently small, the internal dynamics are not effectively allowing the entanglement to characteristically rise. We observe an optimal window where $\tau \approx O(T^{-1})$ in which the Page curve behaviour is categorically observed.

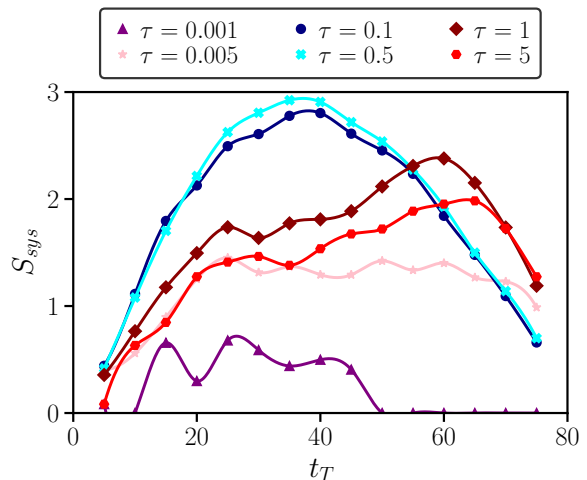


Figure 10. We simulate time evolution of the time independent Hamiltonian \hat{H} through unitary evolution simulated with a TEBD protocol (see Appendix A for more information). The x-axis denotes the time evolution passed, simulated in increments of $\tau = 0.1$ with an evaporation time-step $T = 5$, each marker denotes a point where an evaporation event was performed. When $\frac{t}{T} \in \mathbb{Z}$ the von Neumann entropy is measured, recorded and then an evaporation event is performed. We keep $N = 15$, $M = 150$ and $h = 3$. This is done to ensure $\tau = 0.1$ is a viable choice of time step to simulate the evolution.

[1] W. Israel, Event horizons in static vacuum space-times, Phys. Rev. **164**, 1776 (1967).
 [2] D. C. Robinson, Uniqueness of the kerr black hole, Phys. Rev. Lett. **34**, 905 (1975).
 [3] P. O. Mazur, Proof of uniqueness of the kerr-newman black hole solution, Journal of Physics A: Mathematical and General **15**, 3173 (1982).

[4] R. Ruffini and J. A. Wheeler, Introducing the black hole, Physics Today **24**, 30 (1971).
 [5] S. W. Hawking, Particle creation by black holes, Communications in Mathematical Physics **43** (1975).
 [6] S. W. Hawking, Breakdown of predictability in gravitational collapse, Phys. Rev. D **14**, 2460 (1976).
 [7] S. W. Hawking, Black hole explosions?, Nature **248**, 30 (1974).

- [8] D. N. Page, Is black-hole evaporation predictable?, *Phys. Rev. Lett.* **44**, 301 (1980).
- [9] D. N. Page, Information in black hole radiation, *Phys. Rev. Lett.* **71**, 3743 (1993).
- [10] R. Jha, S. R. Manmana, and S. Kehrein, Page curve and entanglement dynamics in an interacting fermionic chain, *Phys. Rev. B* **111**, 235140 (2025).
- [11] S. Kehrein, Page curve entanglement dynamics in an analytically solvable model, *Phys. Rev. B* **109**, 224308 (2024).
- [12] T. Ray, A. Dhar, and M. Kulkarni, Page curve like dynamics in interacting quantum systems, *Phys. Rev. B* **112**, 174309 (2025).
- [13] L. H. Li, S. Kehrein, and S. Gopalakrishnan, Sharp page transitions in generic hamiltonian dynamics, *Phys. Rev. B* **112**, 014307 (2025).
- [14] F. Ares, S. Scopa, and S. Wald, Entanglement dynamics of a hard-core quantum gas during a joule expansion, *Journal of Physics A: Mathematical and Theoretical* **55**, 375301 (2022).
- [15] R. J. Elliott, P. Pfeuty, and C. Wood, Ising model with a transverse field, *Phys. Rev. Lett.* **25**, 443 (1970).
- [16] R. Mondaini, K. R. Fratus, M. Srednicki, and M. Rigol, Eigenstate thermalization in the two-dimensional transverse field ising model, *Phys. Rev. E* **93**, 032104 (2016).
- [17] R. B. Stinchcombe, Ising-model in a transverse field .1. basic theory, *JOURNAL OF PHYSICS C-SOLID STATE PHYSICS* **6**, 2459 (1973).
- [18] P. Pfeuty, The one-dimensional ising model with a transverse field, *Annals of Physics* **57**, 79 (1970).
- [19] R. J. Elliott and C. Wood, The ising model with a transverse field. i. high temperature expansion, *Journal of Physics C: Solid State Physics* **4**, 2359 (1971).
- [20] P. Pfeuty and R. J. Elliott, The ising model with a transverse field. ii. ground state properties, *Journal of Physics C: Solid State Physics* **4**, 2370 (1971).
- [21] T. Hashizume, I. P. McCulloch, and J. C. Halimeh, Dynamical phase transitions in the two-dimensional transverse-field ising model, *Phys. Rev. Res.* **4**, 013250 (2022).
- [22] T. Kadowaki and H. Nishimori, Quantum annealing in the transverse ising model, *Phys. Rev. E* **58**, 5355 (1998).
- [23] H. Bernien, S. Schwartz, A. Keesling, H. Levine, A. Omran, H. Pichler, S. Choi, A. S. Zibrov, M. Endres, M. Greiner, V. Vuletić, and M. D. Lukin, Probing many-body dynamics on a 51-atom quantum simulator, *Nature* **551**, 579–584 (2017).
- [24] R. Blatt and C. Roos, Quantum simulations with trapped ions, *Nature Physics* **8**, 277 (2012).
- [25] J. Preskill, Quantum computing in the nisq era and beyond, *Quantum* **2**, 79 (2018).
- [26] Y. Sekino and L. Susskind, Fast scramblers, *Journal of High Energy Physics* **2008**, 065 (2008).
- [27] J. Maldacena and D. Stanford, Remarks on the sachdev-ye-kitaev model, *Phys. Rev. D* **94**, 106002 (2016).
- [28] P. Calabrese and J. Cardy, Entanglement entropy and quantum field theory, *Journal of Statistical Mechanics: Theory and Experiment* **2004**, P06002 (2004).
- [29] E. Lieb and D. Robinson, The finite group velocity of quantum spin systems, *Communications in Mathematical Physics* **28**, 251 (1972).
- [30] J. D. Bekenstein, Black holes and entropy, *Phys. Rev. D* **7**, 2333 (1973).
- [31] J. de Jong, F. Hahn, N. Tcholchev, M. Hauswirth, and A. Pappa, Extracting ghz states from linear cluster states, *Physical Review Research* **6**, 013330 (2024).
- [32] R. Orús, A practical introduction to tensor networks: Matrix product states and projected entangled pair states, *Annals of Physics* **349**, 117–158 (2014).
- [33] G. Vidal, Efficient simulation of one-dimensional quantum many-body systems, *Phys. Rev. Lett.* **93**, 040502 (2004).
- [34] M. Suzuki, Generalized trotter’s formula and systematic approximants of exponential operators and inner derivations with applications to many-body problems, *Commun.Math. Phys.* **51**, 182 (1976).
- [35] E. Knill, Quantum computing with realistically noisy devices, *Nature* **434**, 39 (2005).
- [36] T. A. Chowdhury, K. Yu, M. Asaduzzaman, and R. S. Sufian, Capturing the page curve and entanglement dynamics of black holes in quantum computers, *Nuclear Physics B* **1019**, 117112 (2025).
- [37] E. Pelofske, Comparing three generations of d-wave quantum annealers for minor embedded combinatorial optimization problems, *Quantum Science and Technology* **10**, 025025 (2025).
- [38] J. Tindall, M. Fishman, E. M. Stoudenmire, and D. Sels, Efficient tensor network simulation of ibm’s eagle kicked ising experiment, *PRX Quantum* **5**, 010308 (2024).
- [39] A. I. Larkin and Y. N. Ovchinnikov, Quasiclassical method in the theory of superconductivity, *Sov. Phys. JETP* **28**, 1200 (1969).
- [40] S. H. Shenker and D. Stanford, Black holes and the butterfly effect, *Journal of High Energy Physics* **2014**, 67 (2014).
- [41] P. Hosur, X.-L. Qi, D. A. Roberts, and B. Yoshida, Chaos in quantum channels, *Journal of High Energy Physics* **2016**, 4 (2016).
- [42] J. Maldacena, S. H. Shenker, and D. Stanford, A bound on chaos, *Journal of High Energy Physics* **2016**, 106 (2016).
- [43] B. Swingle, G. Bentsen, M. Schleier-Smith, and P. Hayden, Measuring the scrambling of quantum information, *Physical Review A* **94**, 040302 (2016).
- [44] D. A. Roberts and B. Yoshida, Chaos and complexity by design, *Journal of High Energy Physics* **2017**, 121 (2017).
- [45] M. Fishman, S. R. White, and E. M. Stoudenmire, The ITensor Software Library for Tensor Network Calculations, *SciPost Phys. Codebases* , 4 (2022).
- [46] S. R. White, Density matrix formulation for quantum renormalization groups, *Phys. Rev. Lett.* **69**, 2863 (1992).
- [47] S. R. White, Density-matrix algorithms for quantum renormalization groups, *Phys. Rev. B* **48**, 10345 (1993).
- [48] U. Schollwöck, The density-matrix renormalization group, *Rev. Mod. Phys.* **77**, 259 (2005).
- [49] U. Schollwöck, The density-matrix renormalization group in the age of matrix product states, *Annals of Physics* **326**, 96 (2011), january 2011 Special Issue.
- [50] E. R. Davidson, The iterative calculation of a few of the lowest eigenvalues and corresponding eigenvectors of large real-symmetric matrices, *Journal of Computational Physics* **17**, 87 (1975).
- [51] S. R. White and A. E. Feiguin, Real-time evolution using the density matrix renormalization group, *Phys. Rev. Lett.* **93**, 076401 (2004).
- [52] G. Vidal, Efficient classical simulation of slightly entangled quantum computations, *Physical Review Letters*

- 91**, 10.1103/physrevlett.91.147902 (2003).
- [53] N. Hatano and M. Suzuki, Finding exponential product formulas of higher orders, in *Quantum Annealing and*

Other Optimization Methods (Springer Berlin Heidelberg, 2005) p. 37–68.